Spitzer Wide-Area Infrared Extragalactic Survey: Number Counts in the SDSS R-Band

Kye B. Choo

***Abstract*—SDSS r′-band (0.177 eV to 0.216 eV) images covering roughly 0.06 square degrees of sky obtained from part of the SIRTF Wide-Area Infrared Extragalactic (SWIRE) Survey done using the MOSAIC-1 camera on the Spitzer 4.0m telescope from the Kitt Peak National Observatory (KPNO) were catalogued.[1] A total of 1826 sources[2] were identified within the survey field with coordinates (J2000) RA $10^h46^m00.00^s$ to RA $10^h46^m44.20^s$ and DEC $59^\circ01'59.99''$ to DEC $59^\circ21'49.63''$. The number counts were plotted on a semi-log plot of $\log_{10}\mathrm{N}(>\mathrm{r}')$ against r′, and the gradient of the semi-log plot was calculated from our analysis as $0.35^{+0.06}_{-0.07}$, compared to an expected theoretical value of 0.60 for the no-evolution model. Although our calculated power-law constant $\alpha = 0.85^{+0.05}_{-0.05}$ (i.e the gradient of the binned half-magnitudes against magnitudes) deviates significantly from theoretical predictions, further analysis and comparisons with similar surveys done in the r′-band compiled by the Durham Extragalactic Astronomy & Cosmology Research Group [3] shows better agreement ($\alpha_{\mathrm{Durham}} = 0.98^{+0.01}_{-0.01}$). In this report, various methodologies used in our analysis were explored and comments on their effectiveness was given, along with discussions on the results.**

I. Introduction

THE number counts of celestial sources as a function of magnitude is a common cosmological test used to predict the evolution of the universe [4]. Various cosmological models were proposed to explain the evolution of the universe since its formation about 13.8 billion years [5] ago. A basic model would be the no-evolution model, which assumes that (1) the number of galaxies per unit volume in space is conserved after their formation and (2) the luminosities of galaxies is constant over time [6]. To test for the validity of this model, the α factor in the power law relation of the differential number counts against flux could be compared to empirical observations.

During the early years of discovery, the power law was observed to be around $\alpha = 1.50$, which is in excellent agreement with the Euclidean 'no-evolution' model. However, later discoveries also yielded α values that presented strong evidence to argue that this was not the case (see Table I). In this report, a similar analysis was conducted on the data obtained by the KPNO as part of the SWIRE surveys and a value of α was computed. In the following sections, an overview of the underlying theory was presented followed by the methodology and results, before wrapping up the report with a discussion on the results and a final conclusion.

[1]Referring specifically to the Sloan Digital Sky Survey 'r′-band' filter, not to be confused with the Johnson 'R-band' filter.

[2]The term 'sources' will be used throughout this report, even though the term 'galaxies' was used in the lab manual. This is due to technical limitations in the ability to differentiate between stars and galaxies. The decision was made with reference to other published works [1] [2]. Further discussion regarding this could be found in Section V.

α	Survey	Ref.
1.53 ± 0.16	Maccacaro et al. (1982)	[7]
1.50 ± 0.12	Giola et al. (1984)	[8]
1.45 ± 0.12	Giola et al. (1984)	[9]
2.75 ± 0.15	Piccinotti et al. (1982)	[10]
2.25 ± 0.35	Marshall et al. (1983)	[11]
$2.60 - 2.80$[3]	Maccacaro et al. (1982)	[12]

TABLE I: α-values calculated in past surveys. The first three surveys support the no-evolution Euclidean model of the universe, which requires that α be 1.50. However, the next three surveys present strong evidence to reject the no-evolution model.

II. Theory

A. Power Law Relation

Assuming static Euclidean space, uniform large-scale galaxy density, and that luminosities of sources does not vary over time, the luminosity function (LF) of celestial objects could be given by

$$\frac{dN(m)}{dm} \propto 10^{0.6m} \equiv 10^{\beta m}, \tag{1}$$

where $\frac{dN(m)}{dm}$ would be the differential source number counts in each magnitude bins (usually quoted in half-magnitude bins) per solid angle, m would be the magnitude of objects, β would be the gradient of the LogN-m* plot.

A more common expression used for comparing across literature would be the α factor given in the power law relation

$$N(>f) \propto f^{-\frac{3}{2}} \equiv f^{-\alpha}, \tag{2}$$

where N($>f$) is the number of objects with flux exceeding f plotted against flux f.

The derivation of Equation (1) and (2) from the key assumptions is given in Appendix (C-A) along with the derivation of the conversion between α and β

$$\alpha = 2.5\beta. \tag{3}$$

[3]Maccacaro et al. argues that rather than having one single α value, the luminosity function is split into two parts with different α factors for each part.

Under the no-evolution model, Equation (1) and (2) holds and the empirical gradient should be $\alpha = 2.5$ or equivalently $\beta = 0.60$.

B. Seeing the Heat

Astronomical images are normally taken in several filter bandpass. Some common bandpasses are the Johnson UVBRI System and the SDSS u′g′r′i′z′ System. A standardised system allows astronomer to meaningfully compare results across surveys. This survey measured photons of 1.77 eV to 2.16 eV (5750$\mathring{A}$ - 7000$\mathring{A}$) using the SDSS r′-band. The transmission rate of the r′-band is given in Figure (1) below. The Johnson R-band has a similar bandpass at 1.77 eV to 2.48 eV [13] [14] and thus surveys done using the R-band would be included in our discussion.[4]

The images compiled in the survey are done with CCD imaging with an exposure time of 720 seconds.[5] The readings in Analog-Digital Units (ADU) are then converted to magnitudes using the relation (derived in Appendix C-A):

$$m = \text{ZP}_{\text{inst}} - 2.5log_{10}(\text{counts}). \tag{4}$$

The CCD has a maximum good-value of 3600O ADU as given in Table III, Appendix B, therefore any readings above this value would cease to be linear and would be excluded in our later analysis.

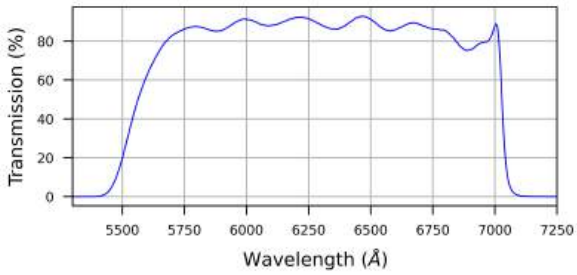

Fig. 1: Passband of the SDSS-r-k1018 filter used in the survey. The data was downloaded from the manufacturer NOIRLab [15] and re-plotted in Python.

III. Construction of the Catalogue

We attempted to catalogue our data using two different methods. The first method would involve identifying sources followed by taking the luminosity and subtracting the background. The second method would involve computing the local background before identifying the sources and computing the luminosity. Both methods would be presented in this section and the results of each would be presented together in Section IV.

A. Annulus Method

When the pixel values within the observation window were binned and a Gaussian was fitted, we found the value of the peak to be 3415.80 ADU with an uncertainty of 0.02 ADU. The sigma of the Gaussian is found to be 12.49 ADU, which upon inspection found that some visually confirmed sources fell within this 1 sigma range from the peak. For the purpose of our analysis, we decided to take the conservative stance and take the peak value of 3415.80 ADU as the background, with noise being σ = 0.02 ADU, positive sources were then defined as pixels having a value of 5σ above the background.[6]

The image as obtained from the FITS file contains problematic features such as saturated pixels and 'blooming' pixels resulting from over-exposure from bright sources. To prepare the image for cataloging, such regions were first identified and removed from the analysis, as shown in Figure 3.

A routine is then defined to identify the brightest pixel within the window, fit two Gaussians across it in the x and y direction, and obtain a fit for σ. The luminosity of the object is then taken to be the sum of all pixels within the circle with a radius of 4σ, and the background would be the average values of the pixels in the annulus bounded by the rings with radius of 4σ to 6σ multiplied by the number of pixels within 4σ. This is summarised by Equation 5 and illustrated by Figure 2. The involved pixels are unflagged and the process is repeated until there is no pixel left with a value 5σ above the background.

$$m' = \sum_{i}^{M} \text{Pix}_i - M \times \sum_{j}^{N} \frac{\text{Pix}_j}{M}, \tag{5}$$

for i in $r < 4\sigma$ and j in $4\sigma < r < 6\sigma$.[7]

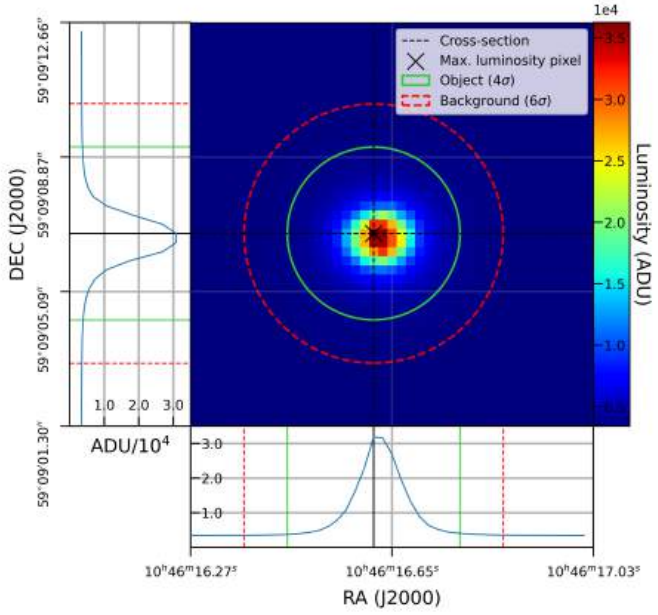

Fig. 2: Illustration of the determination of annulus.

[4]Refer to Figure 10, Appendix D for full comparison of the passbands of different filters.

[5]Refer to Table III, Appendix B.

[6]This estimate of noise is probably too low, leading to the second method in Section III-B.

[7]Further discussion of this method could be found in Appendix E-A.

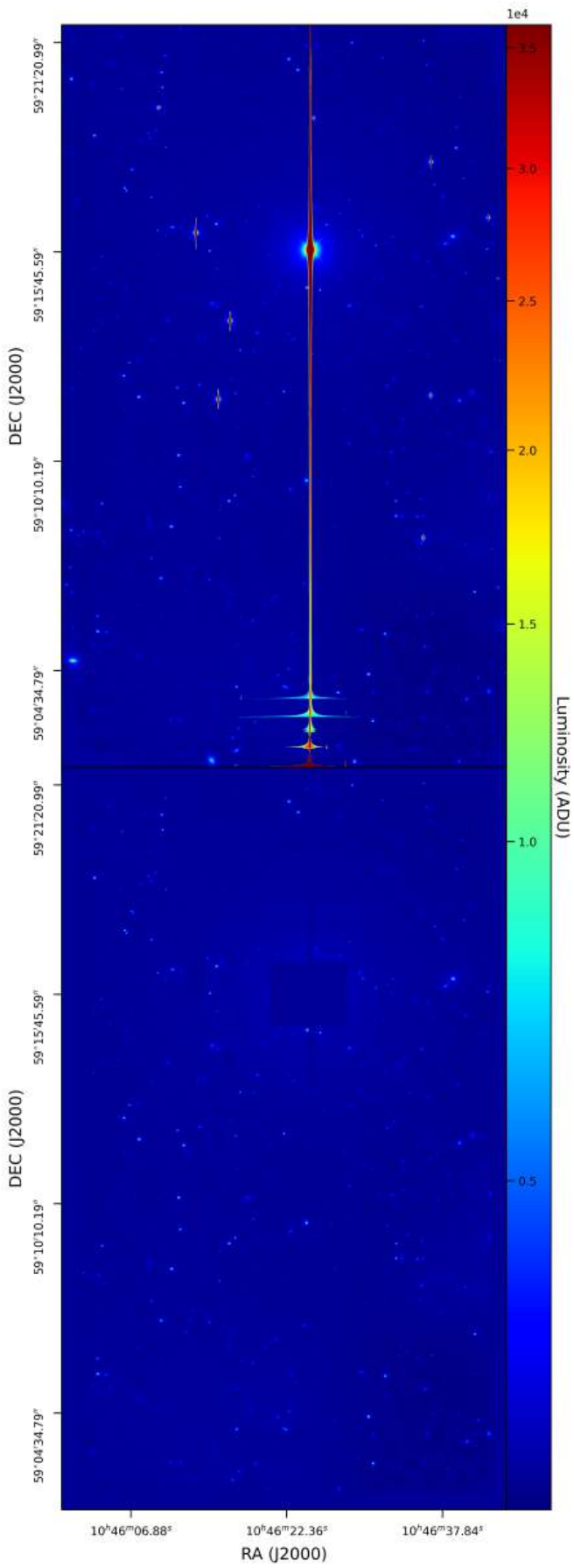

Fig. 3: **LEFT:** Illustration of the field obtained from the KPNO data set. **Top:** image of raw data with features such as 'blooming' sources due to saturation of the pixels (e.g. the vertical red line across the center of the image at about $DEC = 10^h46^m22.36^s$), and bad pixels due to CCD imaging (e.g. near the edges of the field). **Bottom:** the same field after manual removal of these 'problematic' features.

B. Local Background Method

In the second method, the local background for each pixel is first computed with the peak of a histogram made using a 31×31 box of pixel surrounding it, and the σ of a Gaussian fit through the histogram is obtained. If the pixel has a value 5σ higher then the background, it would be flagged for further processing [16]. The result is shown in Figure 4, where it could be observed that the background count actually varies quite significantly throughout the window. Once all pixel has been processed and flagged, it was grouped into objects, where the luminosity is then computed using the pixel values subtracted with the local background that was found for the pixel.

IV. Data and Analysis

To analyse our data, we focused on the data set obtained using the annulus method. The catalogue formed by the methods described in Section 2 were first grouped into half-magnitude bins. We attempted two methods of analysing our data.

First would be to plot our data into a logarithmic form of Equation (2):

$$log_{10}N(< m) = 0.6m \equiv \beta m, \tag{6}$$

where m in the equation would represent the r′ magnitude in our survey and N($< m$) would be the total number of sources brighter then m. The gradient is calculated by fitting a straight line through the region of $12 < r' < 16$. The error in this method would be the sum of contributions from (1) error due to source counts within the magnitude bin given by $\sqrt{n}$, (2) the variation of source counts throughout the window, and (3) variation on the source counts when different σ's were used.

(1) The error contribution from $sqrtn$ is just the error on counting statistics. Since bins at higher magnitudes would have larger counts, the absolute error increases while the relative error decreases.

(2) To compute the variation of source counts throughout the window, the window was separated into four sectors, the total number of sources in each sector was then computed and the standard deviation of the total counts in each windows was calculated.

(3) The Routine was ran at three different sets of σ's for defining the source and background, namely (3σ & 5σ), (4σ & 6σ) and (5σ & 7σ). Three different LogN-m* plots were obtained, and the fractional error were then added.

Evidence of no-evolution model would require a gradient of β = 0.6. The resulting plot shown in Figure 5 yeilds a gradient of $0.35^{+0.06}_{-0.07}$ and does not agree with the theoretical predictions of the no-evolution model.

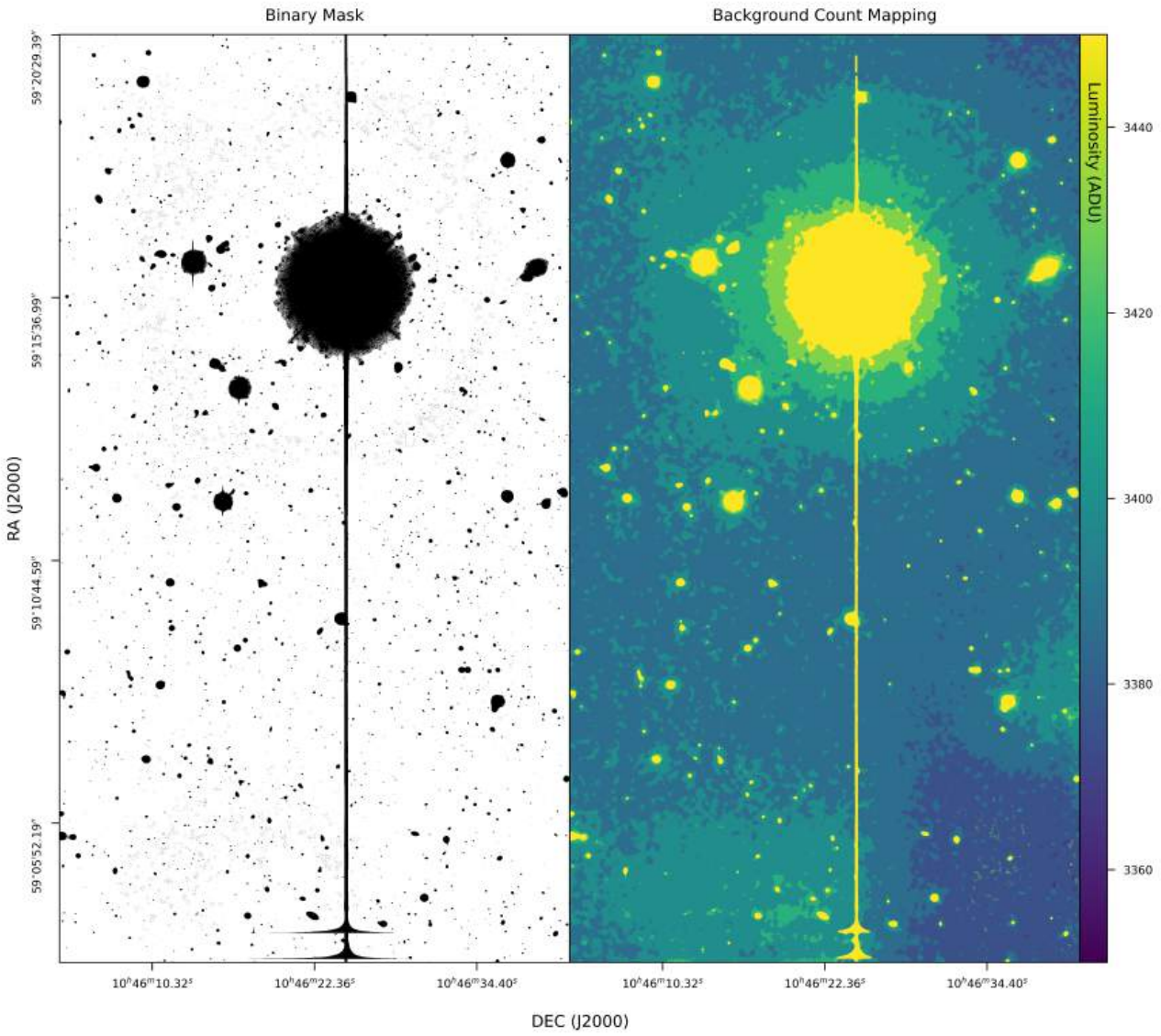

Fig. 4: **Left:** The binary mask with cells set to 1 if the value of the pixel is 5σ's above the background. **Right:** The background count mapping of the window, it could be seen that the background counts varies significantly across the window, which would explain the large width obtained for the Gaussian in the fit for the backgrounds in the annulus method.

A second method of analysing the data was employed to compare our findings with other published works. The binned half-magnitudes was plotted against the magnitudes and this is essentially plotting for Equation (1). A gradient of $0.34^{+0.02}_{-0.02}$ was obtained for the annulus method, and a gradient of $0.29^{+0.02}_{-0.02}$ was obtained for the background method. Although both result does not agree with the no-evolution model's theoretical prediction of 0.6, comparison with data compiled from Durham Physics Cosmology Research Group [3] [17] [18] [19] [20] [21] [22] [23] [24] [25] [26] [27] showed better agreement with a gradient of $0.392^{+0.004}_{-0.004}$. This is illustrated in Figure 6. However, it should be noted that our analysis focuses around the magnitude of $12 < r' < 16$, while the counts from Durham has a higher distribution around the magnitudes of r′ = 20.

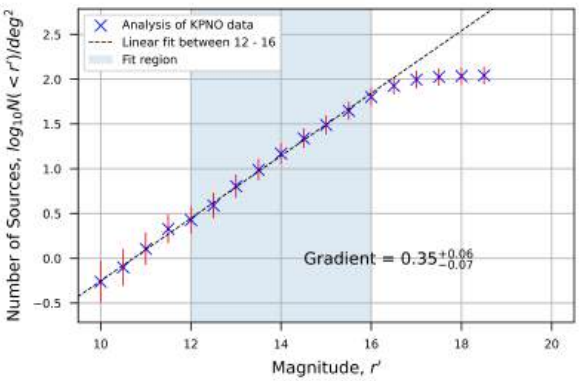

Fig. 5: The LogN($< m$)-r′ plot with gradient obtained by fitting a straight line through $12 < r' < 16$ is 0.35[+0.06, -0.07].

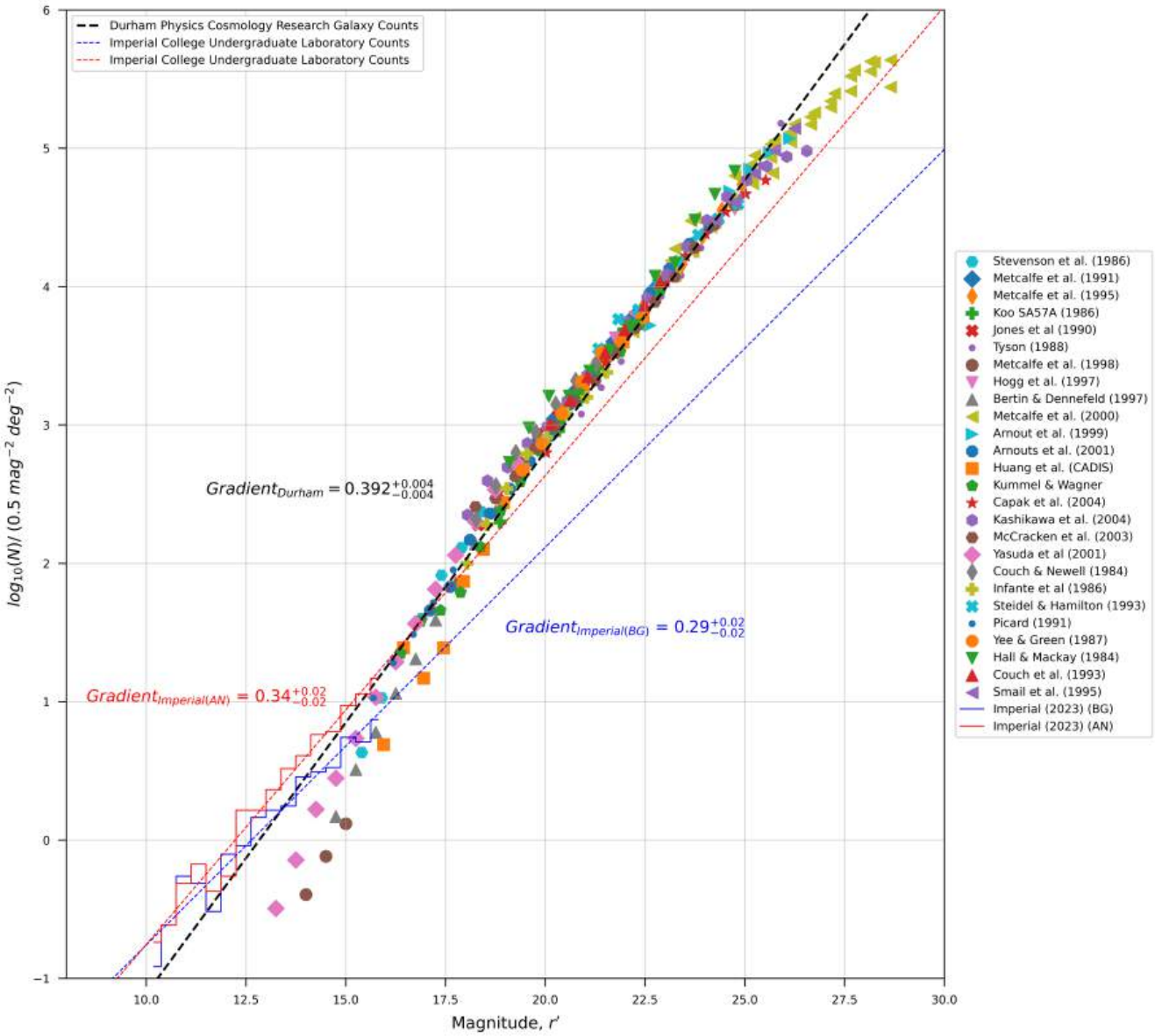

Fig. 6: The above plot shows the data collected using the annulus method and the background method, plotted along with data compiled from Durham Physics Cosmology Research Group [3]. The counts were binned into half$_magnitudesandnormalisedtodeg^{-2}$ in order to ease comparison. It could be seen that the slope agrees to an extent, of around 0.30 - 0.40, rather than the prediction of 0.60, thus validating our methodology. However, note that the Durham counts has a concentration near M $\approx$ 21, while our data was centered around M $\approx$ 14, which could lead to bias. We also found that the annulus method actually matched the results from Durham better, even though the background method was supposed to be an improvement from the annulus method.

V. Discussion

Referring to Table I in Section I, a possible explanation for the discrepancies of the α values could be that each survey might be cataloging different celestial objects. According to Giola et al. (1984) [8] and Maccacaro et al. (1983) [12], the empirically observed α value of 1.50 for the overall universe could just a coincidence due to the sum of number counts from different celestial objects. Further analysis of their catalogues found that active galactic nuclei (AGN) and quasars has a higher α value [9] [11], and that galaxy clusters has a relatively small α value [9] [8]. When surveying data, there could be bias in the number counts, for example samples selected at higher fluxes and energies are dominated by galaxy clusters [7], which could result in different values of α. The value of α = 1.50 in some surveys is the the sum of different contributions from different classes of celestial objects [12].

There luminosity function (Equation (2)) used in our analysis can also be improved by using better models. A possible LF to be used would be the Schechtzer parameterisation given by:

$$\begin{aligned}\Phi(M) =& 0.92\Phi^{\star}\exp\Big[-0.92(\alpha+1)(M-M^{\star}) \\ &- exp{-}0.92(M-M^{\star})\Big]dM\end{aligned} \tag{7}$$

where α is the slope of the LF at the faint end, $M^{\star}$ is the magnitude where the knee of the function occurs, and $\phi^{\star}$ is the number density of galaxies [6]. Referring to Figure 6, it could be seen that the LF could not be exactly fitted with a straight line relation due to the knee (curve) of the function, thus the Schechtzer parameterisation could be a better fit.

For the data obtained from the annulus method, we also found that if we assume the that the radii of the circle used to extract the luminosity was taken to be a dimension of the object, and the arbitrary temperature T* was calculated from the luminosity using the relation:

$$L = 4\pi R^2 \sigma T^{\star 4}, \tag{8}$$

an odd result was returned, This is displayed in Figure 7, where we could see that the relation somehow mimics the Hertzsprung–Russell diagram of a star. There could be further investigation regarding this, particularly regarding whether the luminosity relation given in Equation 8 is purely derived from basic thermodynamic assumptions and could be invariant under different length scales.

VI. Conclusion

In conclusion, our analysis obtained a gradient β of 0.34 ± 0.02 corresponding to an α of 0.85 ± 0.05 in the power-law relation. Although this is not in agreement with the static Euclidean no-evolution model, comparisons to similar publication (= 0.98 ± 0.01) showed agreement to a certain extent, and thus validating our methodology. The discrepancy between the theoretical α and the actual measured alpha could be attributed to the different distribution of celestial objects when observed at different passbands.

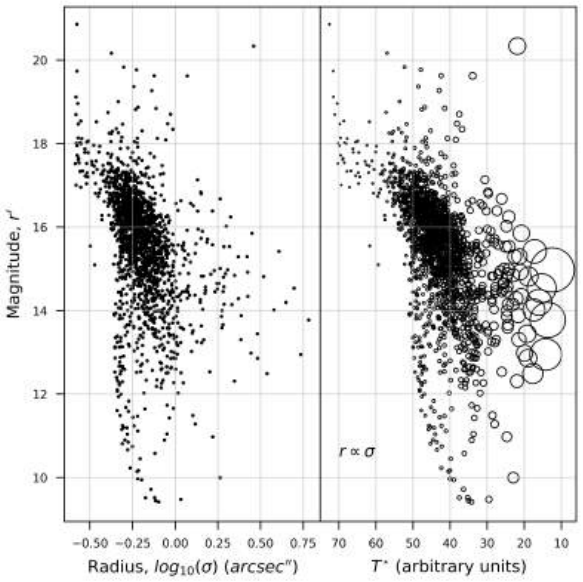

Fig. 7: **Left:** The distributions of magnitudes against radius obtained in our catalogue. **Right:** Assuming that Equation (8) is true for celestial objects, the distributions of magnitudes against an arbitrarily defined temperature. The size of the circle would be representative of the radius of the objects. It could be seen that the general distribution mimics that of the Hertzsprung–Russell diagram, with objects of larger dimensions being more concentrated to the right with higher arbitrary temperatures. This could be a relation to further look into.

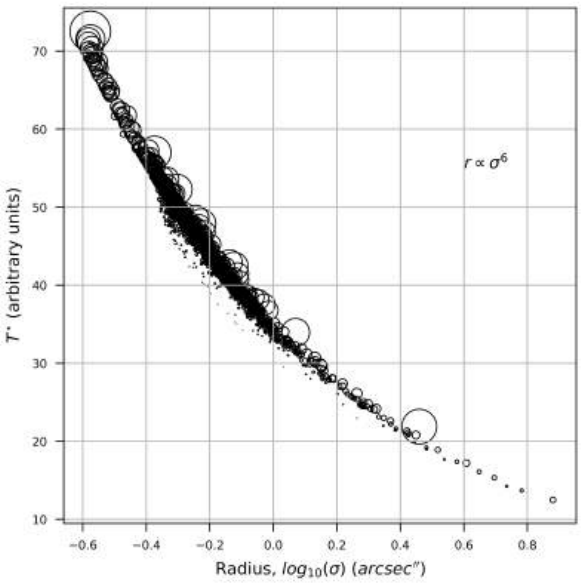

Fig. 8: The same catalogue as Figure 7, but with arbitrary temperatures plotted against radius. It could be seen that it followed a nicely defined curve. The radius of the circles was plotted proportional to magnitudes[6] to highlight the relation against magnitudes. No obvious relation or patterns of distribution of magnitudes are seen in this diagram.

APPENDIX A
FEEDBACK FROM PREVIOUS LAB CYCLES

A. Lab Cycle 1: The Photoelectric Effect

Slides were well constructed with content presented in a clear and concise manner. You made good use of visual aids with correctly formatted tables and figures, the insets in particular were useful to highlight key features in the data. Good background equations and detail of the experiment was provided - although it would have been helpful to spend one or two sentences or a diagram explaining the basic photo-electric effect itself then detail the underlying theory. In-depth analysis sections demonstrated strong technical capabilities. Results comparing the different processing techniques used were insightful. Good automation of set-up. Inclusion of an experimental system diagram would have been helpful to support the preliminary and methodology sections Conclusion slide was more a summary of results but did not express any take-away conclusions. Good to have the suggestions for improvement - maybe re-title slide to "Summary and Suggestions for Improvement" would better match slide content.

B. Lab Cycle 2: Investigating Compton Scattering

The figures included in the report are appropriate with legible axis labels. Fig. 1 includes relevant details and measured distances with errors. It is good that you have given a thought to things which might be improved with the experiment. The description of the different steps of the experiment is too brief, and could be improved with more added details. All variables in the equations should be defined in the text. The report has a lack of numerical results from the measurements.

APPENDIX B
IMPORTANT VALUES OF THE SURVEY

The following key values outlined in Table II and Table III were extracted from the heading section of the FITS file. They contain important information such as the time and coordinates of the observation, and the calibration factor 'ZPT' that could be used as part of the instrumental 'zero-point' in Equation (10) calibration to convert the CCD readings from Analogue-Digital Units to meaningful units of luminous magnitudes in the AB or Vega systems.

Right Ascension of Observation	=	10:46:00.00 (hr)
Decline of Observation	=	59:01:59.99 (deg)
Date (UTC approximate)	=	2002-02-19
Time (UTC approximate)	=	06:12:10.7
Modified Julian Day	=	52324.25845718
Local Sidereal Time[8]	=	8:41:55

TABLE II: Details of the survey.

[8]See: https://astro.dur.ac.uk/ ams/users/lst.html

Coordinate System	=	FK5 (J2000)[9]
Telescope	=	KPNO 4.0m telescope
RA[10] of Telescope	=	10:46:00.00 (hr)
DEC[11] of Telescope	=	59:02:00.0 (deg)
Atm. Dispersion Corr.	=	Mayall Corrector [28]
Detector	=	CCDMosaThin1
Number of CCDs	=	8
Number of Amplifiers	=	8
Pixel Size	=	15 by 15 (microns)
Pixel Scale	=	0.258 by 0.258 (arcsec)
CCD Temperature	=	-1.02599998E+02 (C)
Observation ID	=	kp4m.20020219T061210
Exposure Time	=	720.000 (secs)
Elapsed Time	=	722.287 (secs)
Filter Name	=	r SDSS 1018
Gain (Exp) for Ampr.	=	3.1 (e-/ADU)
Read Noise (Exp) for Ampr.	=	5.6 (e-)
Maximum Good Data Value	=	36000 (ADU)
Photometric Z-Pt.	=	2.530E+01 (mags)
Photometric Z-Pt. Err.	=	2.000E-02 (mags)

TABLE III: Table of telescope settings and specifications relating to the survey.

APPENDIX C
DERIVATION OF KEY RELATIONS

A. The Power Law Relation

Starting off with the equation relating the difference in magnitudes between two sources

$$m_1 - m_2 = -2.5log_{10}(\frac{f_1}{f_2}), \tag{9}$$

where m_1 is the apparent magnitude of the object we are interested in, $m_2 = m_{\text{ref}}$ is a comparison apparent magnitude, and f_1 and $f_2 = f_{\text{ref}}$ is the flux from the observed object and the comparison object respectively.

With a little bit of algebra, we could express Equation (9) as an exponential function of magnitude:

$$\begin{aligned} m_1 &= m_{\text{ref}} + 2.5log_{10}(f_{\text{ref}}) - 2.5log_{10}(f_1) \\ &= \text{ZP}_{\text{inst}} - 2.5log_{10}(f_1), \end{aligned} \tag{10}$$

[9]The J2000 coordinate system in astronomy is a reference frame fixed to the celestial sphere, centered on the mean position of the vernal equinox at the epoch J2000, i.e. the Gregorian calendar date of January 1, 2000, at 12h TT. It provides a stable and standardized framework for expressing celestial coordinates, essential for accurate positional measurements and long-term comparisons of celestial objects.

[10]Right ascension (RA) refers to the east-west direction of a celestial sphere. See: https://science.nasa.gov/learn/basics-of-space-flight/chapter2-2/

[11]Declination (DEC) refers to the north-south direction of a celestial sphere.

$$\therefore\ f_1 = 10^{\frac{2}{5}(-m_1+\text{ZP}_{\text{inst}})} \propto 10^{-0.4m}, \tag{11}$$

where in Equation (10) we have defined a new term $\text{ZP}_{\text{inst}} = m_{\text{ref}} + 2.5log_{10}(f_{\text{ref}})$, which is used as a calibration factor for the instrument.

Assuming static Euclidean space, each unit steradian extends a volume of

$$V = \frac{\frac{4}{3}\pi r^3}{4\pi} = \frac{r^2}{3} \tag{12}$$

from the observation point to the observational limiting distance of r. Further assuming a uniform number density of objects with a specific flux $N(>f)$ in space could be given by n, the total number of visible objects is thus:

$$N(>f) = nV = \frac{nr^3}{3}. \tag{13}$$

Additionally assuming that celestial objects does not evolve and thus has a non-varying flux that could be given by given by

$$f = \frac{L}{4\pi r^2}, \tag{14}$$

substituting into Equation (13), we arrive at the expression

$$\begin{aligned} N(>f) &= \frac{n}{3}(\frac{L}{4\pi f})^{\frac{3}{2}} \\ &= \frac{1}{3}\sum_i n_i(\frac{L_i}{4\pi f})^{\frac{3}{2}}, \end{aligned} \tag{15}$$

$$\therefore\ N(>f) = A_i f^{-\frac{3}{2}} \propto f^{-\alpha}, \tag{16}$$

where in the second line we have categorised the magnitudes into bins (the common convention is to use half-magnitude bins of 0.5 mag^{-1}), and in the third line, we have defined the power law relation to be .

Finally, combining Equation (11) and Equation (15) gives us the expressions

$$N(<m) \propto 10^{0.6m}, \tag{17}$$

$$\frac{dN(m)}{dm} \propto 10^{0.6m}, \tag{18}$$

where Equation (17) is the cumulative number of sources with magnitudes smaller (more luminous) than m, and Equation (18) would be the binned number of sources in each half-magnitudes (using half-magnitude bins are just a convention) [29].

From Equation (11) and Equation (16), it is easy to convert the gradients in LogN-LogS graphs for comparisons to the gradients in LogN-m* by using the relation

$$\begin{aligned} N(>f) &\propto f^{-\alpha} \\ &\propto 10^{-0.4m\alpha}, \end{aligned} \tag{19}$$

$$\begin{aligned} log(N(>f)) &= 0.4\alpha m = \beta m \\ \therefore \alpha &= 2.5\beta, \end{aligned} \tag{20}$$

where we have defined β as the gradient obtained from the semi-log plot of LogN-m*. The purpose of going through the laborious proof of converting the gradient β to α is because most comparison literature was quoted this way.

Following from Equation (10) and Equation (15), the proportionality constant for the power law (or the vertical shift in the LogN-m* relation) could be given by

$$\frac{n_i}{3}\frac{L_i}{4\pi} \times \exp(-\frac{6}{10}m_{\text{ref}}) \times (f_{\text{ref}})^{\frac{5}{2}}. \tag{21}$$

Since m_{ref} and f_{ref} are calibration constants, n is constant throughout all solid angles in the Euclidean uniform density assumption, and objects in the same calibrated magnitude bins should have roughly the same luminosities L_i, the proportionality constant in the power law is only affected by the sensitivities and limitations of the survey. Thus the gradients of the log-plots for Equation (17) and (18) should be independent of instrumental sensitivities and limitation, allowing us to easily compare the α and β constants across surveys.[12] [13]

B. Coordinates of the survey

The FITS file does not have a coordinate directly associated with each pixel. However, the header does contain important information for which the coordinates could be calculated. The coordinate of the survey is given in J2000 celestial coordinates (with reference frame fixed at the Gregorian calendar date of 1^{st} January 2000, 1200 midday TT) and was shown in Table III along with the information regarding the scaling of pixel dimensions to arc-seconds.

The zero-coordinate is given by:

$$\begin{aligned} \text{RA} &= 10:46:00.00 \quad \text{(hr)} \\ \text{DEC} &= 59:01:59.99 \quad \text{(deg)} \end{aligned} \tag{22}$$

To interpret the coordinates, Right Ascension (RA) could be though of as the east-west direction along the longitudinal lines, and the Declination (DEC) could be thought of as the angle subtended from the equator. This is illustrated in Figure (9) extracted from SDSS's website [30].

Since the coordinates are angular, each unit angle would have a different corresponding length for the RA coordinates. An element of RA = 1 hour would be far greater at the equator than near the poles. To convert the coordinates, the following steps are done in code:

[12] Note that the gradient of the LogN-m* plot would still be dependent on the bandpass which the flux of the object is measured.

[13] Also note that the models and assumptions made about the luminosity function must be the same. Other better parameterisation of the LF function exists, such as the Schechter LF which is more commonly used in recent publications.

Each pixel has a dimension of 0.258 × 0.258 arc-seconds. To convert this to degrees:

$$\frac{\text{RA/DEC}}{\text{pixel}} = 0.258\left[\frac{arcsec}{pixel}\right] \times \frac{1}{60}\left[\frac{arcmin}{arcsec}\right] \times \frac{1}{60}\left[\frac{deg}{arcmin}\right] = \frac{0.258}{3600}\left[\frac{deg}{pixel}\right]. \tag{23}$$

Given our image of 4611 × 2570 pixels, the total square degrees is calculated to be 6.09×10^{-2} deg^2 $\equiv 1.85\times10^{-5}$ sr.

The difficult part is to map the pixel dimensions back to RA and DEC. To do this, the DEC is first computed using the modulus-60 system, where each degree is 60 arc-minute and each arc-minute is 60 arc-seconds. However, the conversion of degrees to RA coordinates would be less direct. The RA is defined as having 24 hours in 360 degrees, and 60 minutes in and hour, and 60 seconds in each minute. But since the separation of two objects at different DEC with the same RA correspond to different length, e.g. two objects separated by 1 degree of RA near the equator and poles have different lengths, the RA needs to be corrected with the cosine of the DEC.

APPENDIX D
OTHER SUPPORTING REFERENCES

Figure 10 shows how the bandpasses of different systems compare, and that the Johnson R-band is roughly similar to the SDSS r′-band and thus it should not be too big of an issue when comparing data obtained with the two.

APPENDIX E
FURTHER DISCUSSION ON EFFECTIVENESS OF METHODOLOGY

A. Annulus Method

In the annulus method, aside from the estimate of background noise being not ideal, another possible issue might arise from the discrete natures of pixel dimensions r_{pixel} and its behaviour when parameterising them with linear radii $r^\dagger$. To illustrate this, Figure 11 shows that the fractional error on the area is far larger when dealing with small $r^\dagger$ due to the rounding of r_{pixel}, but as $r^\dagger \to \infty$, $r_{\text{pixel}} \to r^\dagger$. The third pane shows the distributions of r_{pixel} of the identified objects and that most of them are centered around 2 - 3 and thus this would not be a big problem.

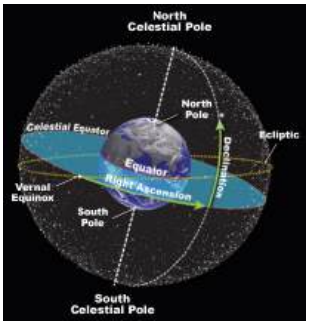

Fig. 9: Diagram illustrating how the celestial coordinates are framed.

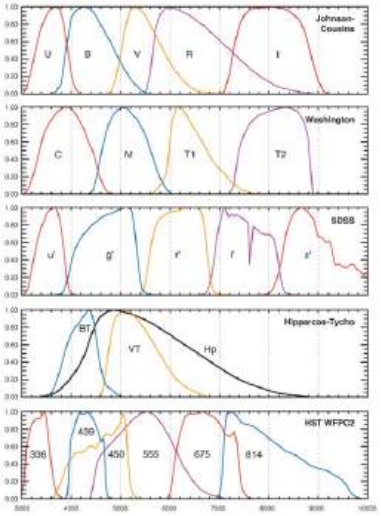

Fig. 10: Comparison of the passband of different photometry system. It could be seen that the SDSS r′-band has a passband similar to that of the Johnson R-band. The image was extracted from 'Standard Photometry Systems', Bessell (2005) [31].

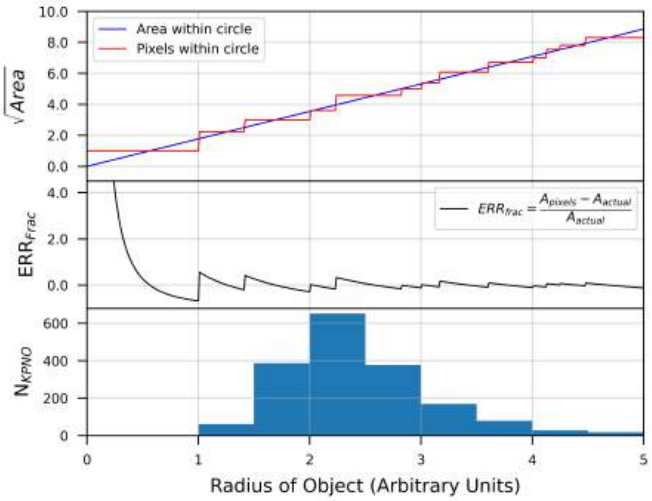

Fig. 11: It could be seen that the fractional error is higher at low radius for the annulus method. However, since most objects identified is of higher radii, this should not be too much of a problem for our analysis.

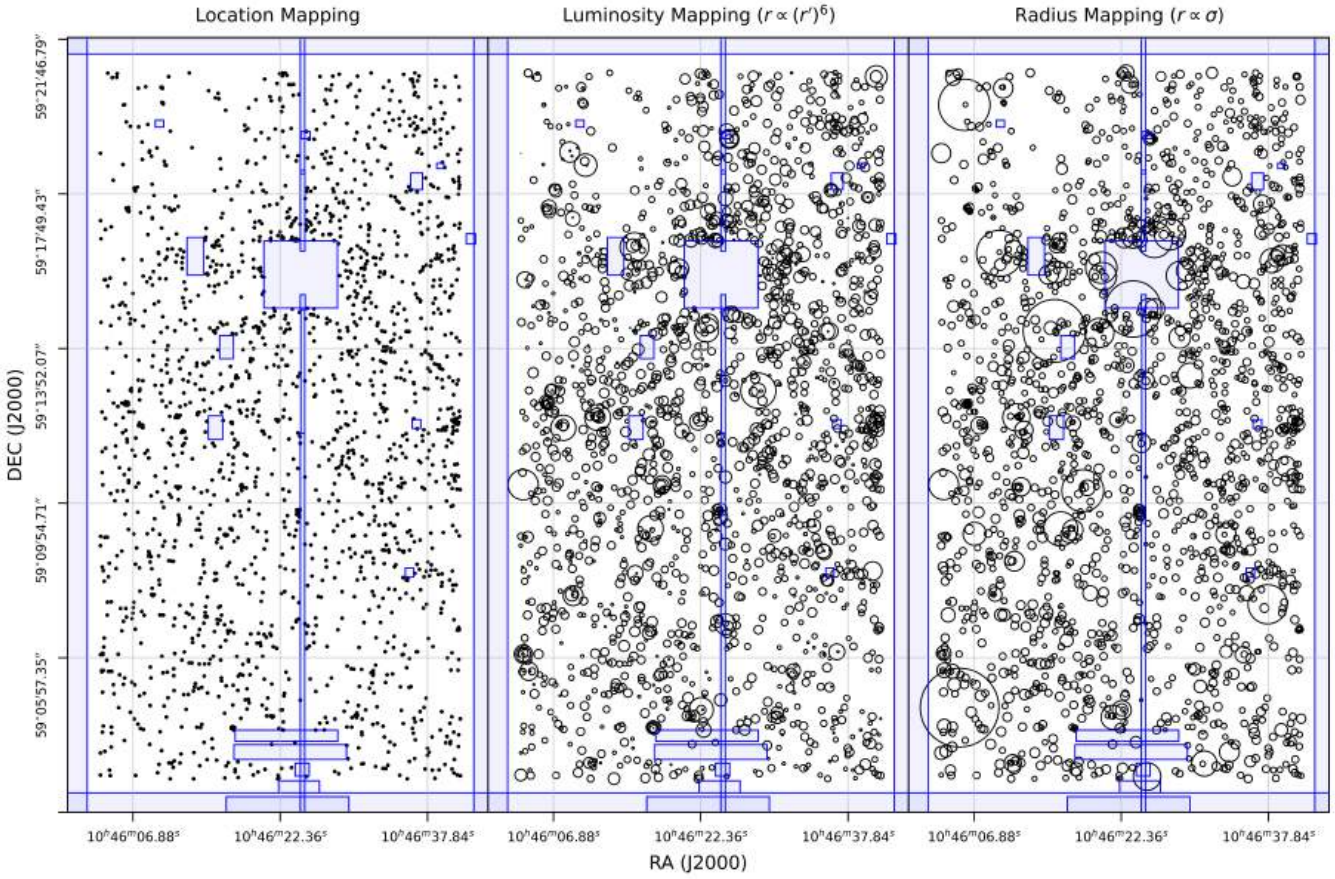

Fig. 12: A mapping of the identified objects using the anulus method. It could be seen that there is no concentration of objects near a region or any particularily odd features. This could thus be used to validate the methodology. The blue boxed in the fugures represent regions excluded from our analysis due to oversaturation.

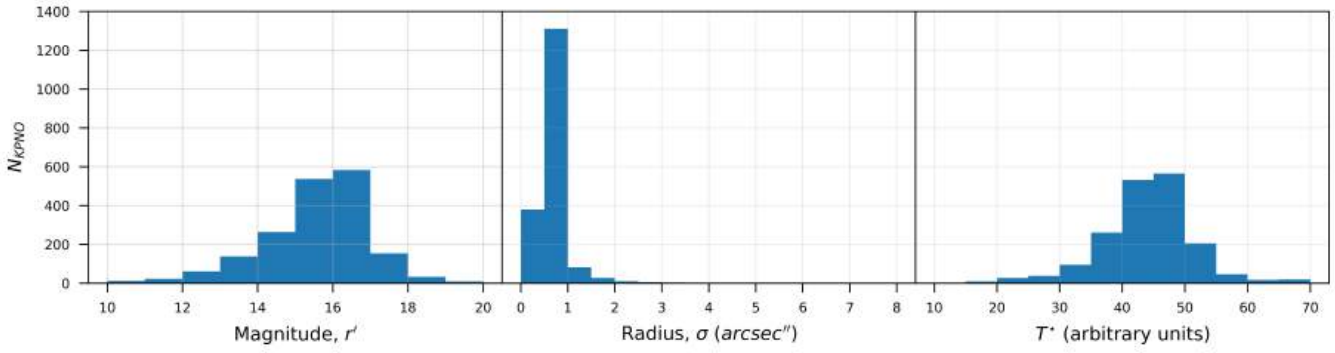

Fig. 13: **Left:** The distribution of magnitudes measured for the sources are centered around r′ = 16 with a longer tail towards lower magnitudes, indicating that the methodology used is able to identify bright objects better than faint ones. **Center:** the radii parameter was seen to be quite concentrated near the region of σ = 1 arcsecs, with only a few measuring up to 8 arcsecs away. **Right:** Assuming that we could calculate an apparent temperature of the object, we could see that it roughly follows a normal distribution.

REFERENCES

[1] D. Fadda, B. T. Jannuzi, A. Ford, and L. J. Storrie-Lombardi, "The Spitzer Space Telescope First-Look Survey: KPNO MOSAIC-1 R-Band Images and Source Catalogs," *The Astronomical Journal*, vol. 128, no. 1, pp. 1–15, 2004.

[2] C. Lonsdale, H. Smith, M. Rowan-Robinson, J. Surace, D. Shupe, C. Xu, S. Oliver, D. Padgett, F. Fang, T. Conrow, A. Franceschini, N. Gautier, M. Griffin, P. Hacking, F. Masci, G. Morrison, J. O'Linger, F. Owen, I. Pérez-Fournon, M. Pierre, R. Puetter, G. Stacey, S. Castro, M. Del Carmen Polletta, D. Farrah, T. Jarrett, D. Frayer, B. Siana, T. Babbedge, S. Dye, M. Fox, E. Gonzalez-Solares, M. Salaman, S. Berta, J. Condon, H. Dole, and S. Serjeant, "Swire: The sirtf wide-area infrared extragalactic survey," *Publications of the Astronomical Society of the Pacific*, vol. 115, no. 810, pp. 897–927, 2003.

[3] [Online]. Available: http://star-www.dur.ac.uk/~nm/pubhtml/counts/counts.html

[4] N. Yasuda, M. Fukugita, V. K. Narayanan, R. H. Lupton, I. Strateva, M. A. Strauss, Ivezić, R. S. J. Kim, D. W. Hogg, D. H. Weinberg, K. Shimasaku, J. Loveday, J. Annis, N. A. Bahcall, M. Blanton, J. Brinkmann, R. J. Brunner, A. J. Connolly, I. Csabai, M. Doi, M. Hamabe, S.-I. Ichikawa, T. Ichikawa, D. E. Johnston, G. R. Knapp, P. Z. Kunszt, D. Q. Lamb, T. A. McKay, J. A. Munn, R. C. Nichol, S. Okamura, D. P. Schneider, G. P. Szokoly, M. S. Vogeley, M. Watanabe, and D. G. York, "Galaxy number counts from the sloan digital sky survey commissioning data," *The Astronomical journal*, vol. 122, no. 3, pp. 1104–1124, 2001.

[5] Planck Collaboration, Aghanim, N., Akrami, Y., Ashdown, M., Aumont, J., Baccigalupi, C., Ballardini, M., Banday, A. J., Barreiro, R. B., Bartolo, N., Basak, S., Battye, R., Benabed, K., Bernard, J.-P., Bersanelli, M., Bielewicz, P., Bock, J. J., Bond, J. R., Borrill, J., Bouchet, F. R., Boulanger, F., Bucher, M., Burigana, C., Butler, R. C., Calabrese, E., Cardoso, J.-F., Carron, J., Challinor, A., Chiang, H. C., Chluba, J., Colombo, L. P. L., Combet, C., Contreras, D., Crill, B. P., Cuttaia, F., de Bernardis, P., de Zotti, G., Delabrouille, J., Delouis, J.-M., Di Valentino, E., Diego, J. M., Doré, O., Douspis, M., Ducout, A., Dupac, X., Dusini, S., Efstathiou, G., Elsner, F., Enßlin, T. A., Eriksen, H. K., Fantaye, Y., Farhang, M., Fergusson, J., Fernandez-Cobos, R., Finelli, F., Forastieri, F., Frailis, M., Fraisse, A. A., Franceschi, E., Frolov, A., Galeotta, S., Galli, S., Ganga, K., Génova-Santos, R. T., Gerbino, M., Ghosh, T., González-Nuevo, J., Górski, K. M., Gratton, S., Gruppuso, A., Gudmundsson, J. E., Hamann, J., Handley, W., Hansen, F. K., Herranz, D., Hildebrandt, S. R., Hivon, E., Huang, Z., Jaffe, A. H., Jones, W. C., Karakci, A., Keihänen, E., Keskitalo, R., Kiiveri, K., Kim, J., Kisner, T. S., Knox, L., Krachmalnicoff, N., Kunz, M., Kurki-Suonio, H., Lagache, G., Lamarre, J.-M., Lasenby, A., Lattanzi, M., Lawrence, C. R., Le Jeune, M., Lemos, P., Lesgourgues, J., Levrier, F., Lewis, A., Liguori, M., Lilje, P. B., Lilley, M., Lindholm, V., López-Caniego, M., Lubin, P. M., Ma, Y.-Z., Macías-Pérez, J. F., Maggio, G., Maino, D., Mandolesi, N., Mangilli, A., Marcos-Caballero, A., Maris, M., Martin, P. G., Martinelli, M., Martínez-González, E., Matarrese, S., Mauri, N., McEwen, J. D., Meinhold, P. R., Melchiorri, A., Mennella, A., Migliaccio, M., Millea, M., Mitra, S., Miville-Deschênes, M.-A., Molinari, D., Montier, L., Morgante, G., Moss, A., Natoli, P., Nørgaard-Nielsen, H. U., Pagano, L., Paoletti, D., Partridge, B., Patanchon, G., Peiris, H. V., Perrotta, F., Pettorino, V., Piacentini, F., Polastri, L., Polenta, G., Puget, J.-L., Rachen, J. P., Reinecke, M., Remazeilles, M., Renzi, A., Rocha, G., Rosset, C., Roudier, G., Rubiño-Martín, J. A., Ruiz-Granados, B., Salvati, L., Sandri, M., Savelainen, M., Scott, D., Shellard, E. P. S., Sirignano, C., Sirri, G., Spencer, L. D., Sunyaev, R., Suur-Uski, A.-S., Tauber, J. A., Tavagnacco, D., Tenti, M., Toffolatti, L., Tomasi, M., Trombetti, T., Valenziano, L., Valiviita, J., Van Tent, B., Vibert, L., Vielva, P., Villa, F., Vittorio, N., Wandelt, B. D., Wehus, I. K., White, M., White, S. D. M., Zacchei, A., and Zonca, A., "Planck 2018 results - vi. cosmological parameters," *AA*, vol. 641, p. A6, 2020. [Online]. Available: https://doi.org/10.1051/0004-6361/201833910

[6] A. Campos, "Galaxy number counts," 1995.

[7] T. Maccacaro, E. D. Feigelson, M. Fener, R. Giacconi, I. M. Gioia, R. E. Griffiths, S. S. Murray, G. Zamorani, J. Stocke, and J. Liebert, "A medium sensitivity X-ray survey using the Einstein Observatory : the log N-log S relation for extragalactic X-ray sources." , vol. 253, pp. 504–511, Feb. 1982.

[8] D. Fadda, B. T. Jannuzi, A. Ford, and L. J. Storrie-Lombardi, "The spitzer space telescope first-look survey: Kpno mosaic-1 r-band images and source catalogs," *The Astronomical journal*, vol. 128, no. 1, pp. 1–15, 2004.

[9] I. M. Gioia, T. Maccacaro, R. E. Schild, J. T. Stocke, J. W. Liebert, I. J. Danziger, D. Kunth, and J. Lub, "The medium sensivity survey : a new sample of X-ray sources with optical identifications and the revised extragalactic log N-log S." , vol. 283, pp. 495–511, Aug. 1984.

[10] G. Piccinotti, R. F. Mushotzky, E. A. Boldt, S. S. Holt, F. E. Marshall, P. J. Serlemitsos, and R. A. Shafer, "A complete X-ray sample of the high-latitude (b)-20 sky from HEAO 1 A-2 : log N-log S and luminosity functions." , vol. 253, pp. 485–503, Feb. 1982.

[11] H. L. Marshall, H. Tananbaum, G. Zamorani, J. P. Huchra, A. Braccesi, and V. Zitelli, "Optical and X-ray observations of faint quasars in an optically selected sample." , vol. 269, pp. 42–48, Jun. 1983.

[12] T. Maccacaro, I. M. Gioia, Y. Avni, P. Giommi, R. E. Griffiths, J. Liebert, J. Stocke, and J. Danziger, "The cosmological evolution and luminosity function of X-ray selected active galactic nuclei," , vol. 266, pp. L73–L77, Mar. 1983.

[13] H. L. Johnson and W. W. Morgan, "Fundamental stellar photometry for standards of spectral type on the Revised System of the Yerkes Spectral Atlas." , vol. 117, p. 313, May 1953.

[14] J. Agar, "The measurement of starlight: Two centuries of astronomical photometry," *Technology and Culture*, vol. 39, no. 4, pp. 764–766, 1998.

[15] Feb 2021. [Online]. Available: https://noirlab.edu/science/filters/kp1018

[16] D. Clements, E. Rigby, S. Maddox, L. Dunne, A. Mortier, C. Pearson, A. Amblard, R. Auld, M. Baes, D. Bonfield, D. Burgarella, S. Buttiglione, A. Cava, A. Cooray, A. Dariush, G. De Zotti, S. Dye, S. Eales, D. Frayer, J. Fritz, J. Gardner, J. Gonzalez-Nuevo, D. Herranz, E. Ibar, R. Ivison, M. Jarvis, G. Lagache, L. Leeuw, M. Lopez-Caniego, M. Negrello, E. Pascale, M. Pohlen, G. Rodighiero, S. Samui, S. Serjeant, B. Sibthorpe, D. Scott, D. Smith, P. Temi, M. Thompson, I. Valtchanov, P. Van der Werf, and A. Verma, "Herschel-atlas: Extragalactic number counts from 250 to 500 microns," 2010-Jul.

[17] L. R. Jones, R. Fong, T. Shanks, R. S. Ellis, and B. A. Peterson, "Galaxy number counts. - I. Photographic observations to B=23.5 mag." , vol. 249, pp. 481–497, Apr. 1991.

[18] N. Metcalfe, T. Shanks, R. Fong, and L. R. Jones, "Galaxy number counts - II. CCD observations to B = 25 mag." , vol. 249, pp. 498–522, Apr. 1991.

[19] N. Metcalfe, T. Shanks, R. Fong, and N. Roche, "Galaxy number counts - III. Deep CCD observations to B=27.5 mag," , vol. 273, no. 2, pp. 257–276, Mar. 1995.

[20] N. Metcalfe, T. Shanks, A. Campos, R. Fong, and J. P. Gardner, "Galaxy formation at high redshifts," , vol. 383, no. 6597, pp. 236–239, Sep. 1996.

[21] H. J. McCracken, N. Metcalfe, T. Shanks, A. Campos, J. P. Gardner, and R. Fong, "Galaxy number counts - IV. Surveying the Herschel Deep Field in the near-infrared," , vol. 311, no. 4, pp. 707–718, Feb. 2000.

[22] N. Metcalfe, T. Shanks, A. Campos, H. J. McCracken, and R. Fong, "Galaxy number counts - V. Ultradeep counts: the Herschel and Hubble Deep Fields," , vol. 323, no. 4, pp. 795–830, May 2001.

[23] W. J. Frith, G. S. Busswell, R. Fong, N. Metcalfe, and T. Shanks, "The local hole in the galaxy distribution: evidence from 2MASS," *Monthly Notices of the Royal Astronomical Society*, vol. 345, no. 3, pp. 1049–1056, 11 2003. [Online]. Available: https://doi.org/10.1046/j.1365-8711.2003.07027.x

[24] G. S. Busswell, T. Shanks, W. J. Frith, P. J. Outram, N. Metcalfe, and R. Fong, "The local hole in the galaxy distribution: new optical evidence," , vol. 354, no. 4, pp. 991–1004, Nov. 2004.

[25] N. Metcalfe, T. Shanks, P. M. Weilbacher, H. J. McCracken, R. Fong, and D. Thompson, "Galaxy number counts - vi. an h-band survey of the herschel deep field: Galaxy number counts - vi. an h-band survey of the whdf," *Monthly Notices of the Royal Astronomical Society*, vol. 370, no. 3, p. 1257–1273, Jun. 2006. [Online]. Available: http://dx.doi.org/10.1111/j.1365-2966.2006.10534.x

[26] D. J. Farrow, S. Cole, N. Metcalfe, P. W. Draper, P. Norberg, S. Foucaud, W. S. Burgett, K. C. Chambers, N. Kaiser, R. P. Kudritzki, E. A. Magnier, P. A. Price, J. L. Tonry, and C. Waters, "Pan-STARRS1: Galaxy clustering in the Small Area Survey 2," *Monthly Notices of the Royal Astronomical Society*, vol. 437, no. 1, pp. 748–770, 11 2013. [Online]. Available: https://doi.org/10.1093/mnras/stt1933

[27] T. Shanks, N. Metcalfe, B. Chehade, J. R. Findlay, M. J. Irwin, E. Gonzalez-Solares, J. R. Lewis, A. K. Yoldas, R. G. Mann, M. A. Read, E. T. W. Sutorius, and S. Voutsinas, "The VLT Survey Telescope ATLAS," , vol. 451, no. 4, pp. 4238–4252, Aug. 2015.

[28] G. H. Jacoby, M. Liang, D. Vaughnn, R. Reed, and T. Armandroff, "New wide-field corrector for the Kitt Peak Mayall 4-m telescope," in *Optical Astronomical Instrumentation*, ser. Society of Photo-Optical Instrumentation Engineers (SPIE) Conference Series, S. D'Odorico, Ed., vol. 3355, Jul. 1998, pp. 721–734.

[29] P. J. E. P. J. E. Peebles, *Principles of physical cosmology*, ser. Princeton series in physics. Princeton, New Jersey: Princeton University Press, 1993 - 1993.
[30] [Online]. Available: https://voyages.sdss.org/preflight/locating-objects/ra-dec/
[31] M. S. Bessell, "Standard photometric systems," *Annual Review of Astronomy and Astrophysics*, vol. 43, no. 1, pp. 293–336, 2005. [Online]. Available: https://doi.org/10.1146/annurev.astro.41.082801.100251